Aida S. Rakhimzhanova[1] , Ruslan A. Muzaparov[1] , Irina A. Pustolaikina[1*] ,
Alfiya F. Kurmanova[1] , Sergey N. Nikolskiy[1] , Darya D. Kapishnikova[2] ,
Alena L. Stalinskaya[3] , Ivan V. Kulakov[3]

[1]Department of Physical and Analytical Chemistry, Karaganda Buketov University, Karaganda, Kazakhstan;
[2]Institute of Chemistry, Saint Petersburg State University, Saint Petersburg, Russia;
[3]Higher School of Natural Science, University of Tyumen, Tyumen, Russia
*(*Corresponding author's e-mail: ipustolaikina@gmail.com)*

A Series of Novel Integrastatins Analogues:
In silico Study of Physicochemical and Bioactivity Parameters

Integrastatins are naturally occurring heterotetracyclic compounds with a broad spectrum of biological activity. A number of new structural analogues of integrastatins **2a-u** have been synthesized using a novel one-step method [1], but a systematic theoretical study of their structural features and biological activity has not been realized. This study aimed to in silico investigate physicochemical and bioactivity properties for a series of 21 new synthetic analogues of natural integrastatins. Global chemical reactivity descriptors was assessed using DFT B3LYP 6-311++G(d, p) CPCM (solvent — water) calculations. High ionization potential IP in the range from 5.9 to 7.1 eV and electron affinity EA at the level of 2.1 to 3.2 eV were shown, which together with a sufficiently large energy gap ΔE_{gap} from 3.8 to 4.6 eV indicates the hard nature of the compounds **2a-u**. Antiviral activity and inhibitory potential as CYP2C19 inducers were identified using the PASSOnline resource. According to the results of molecular docking studies Human immunodeficiency virus HIV-1 reverse transcriptase protein (PDB ID: 3V81) and protein of the RNA-dependent RNA polymerase of the SARS-CoV-2 (PDB ID: 7AAP) can serve as a likely biological target for the compounds **2a-u**. Potentially high oral efficacy and a promising safety profile for the therapeutic use were showed using ADMETlab 3.0 online portal. Further experimental in vitro and in vivo studies of the pharmaceutical potential of compounds **2a-u** is need for more accurate evaluation the assumptions made on the basis of in silico approach.

Keywords: integrastatins, in silico, molecular docking, computational study, biological activity, ADMET, quantum chemical calculations, DFT, B3LYP, antiviral activity, global chemical reactivity descriptors, HIV-1, SARS-CoV-2.

1 Introduction

Integrastatins A, B are organic heterotetracyclic compounds containing a novel four-6′-ring system with an epoxybenzooxocine moiety (Fig. 1). They have a natural origin and are aromatic ethers, bridged compounds, cyclic ethers, a cyclic ketones, organic heterotetracyclic compounds, polyphenols and primary alcohols with a wide range of biological activity, including antiviral, antioxidant, antitumor, antifungal and antimicrobial properties [2].

Integrastatin A   Integrastatin B

Figure 1 Structural formulas of integrastatins

Integrastatin A and integrastatin B were first isolated in 2002 from the ATCC74478 and *Cytospora sp.* fungus, also their inhibitory activity at micromolar concentrations in the strand transfer reaction of recombinant HIV-1 integrase was shown [3]. These compounds immediately emerged as attractive targets for medicinal chemistry due to their antiviral potential, which integrase inhibitors have for the development of HIV

therapy. However, the use of integrastatins obtained by fungal fermentations was limited due to their low content in natural sources and the high cost of the resulting product. Therefore, chemical synthesis as a method that allows obtaining integrastatins in any quantities and with a high degree of purity has received its development. Several research groups have reported different methods of synthesis of the tetracyclic core of integrastatins in the subsequent decades [4–7]. Each of these methods has its own characteristics and advantages, and it should be noted that interest in this type of compounds encourages many chemists to further develop approaches to the synthesis of integrastatins [8–11].

Recent years, the research group of Professor I.V. Kulakov in University of Tyumen (Tyumen, Russia) has developed and repeatedly tested a new method for the one-stage synthesis of structural analogues of the integrastatin tetracyclic core [12–14] (Fig. 2).
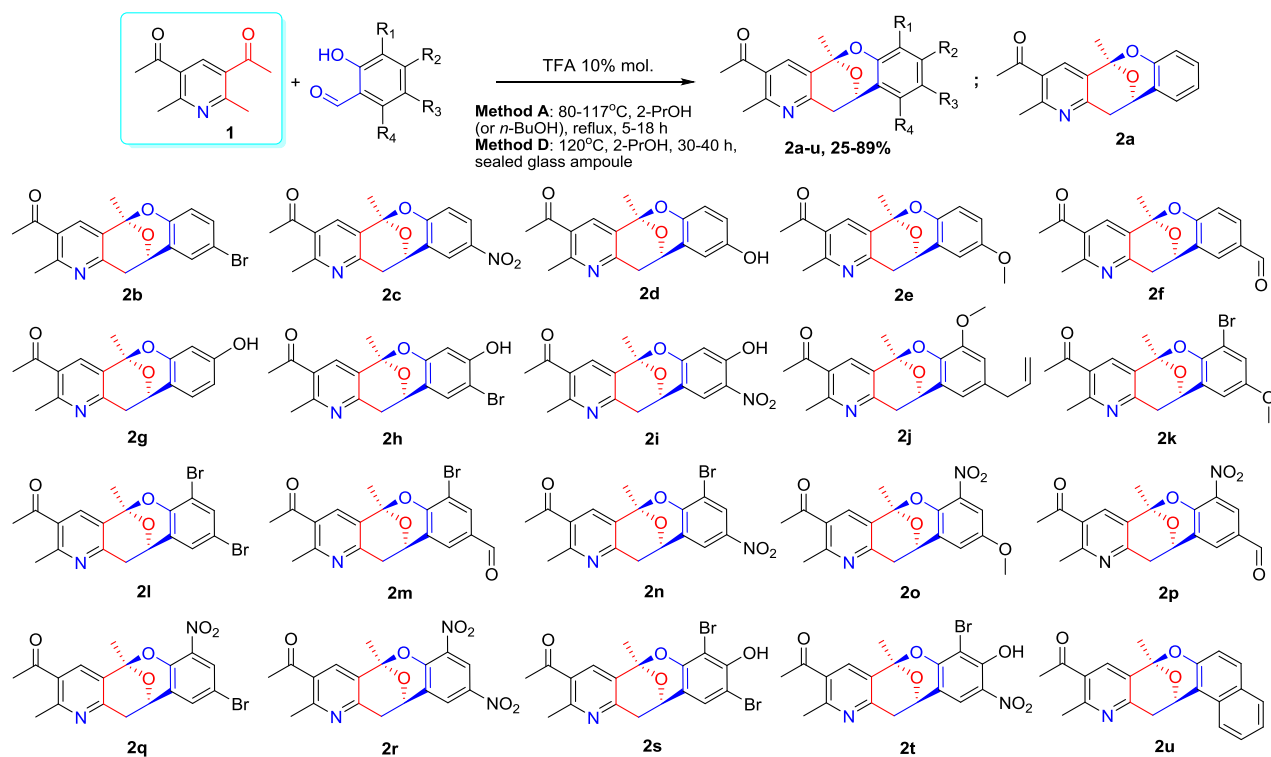

Figure 2. Scheme of synthesis of novel integrastatins analogues **2a-u** [1]

Thus, more than 20 new derivatives of oxocinopyridine **2a-u** with a basic oxocine pharmacophore ring were obtained on the base of 3,5-diacetyl-2,6-dimethylpyridine **1** as a precursor [1]. However, a systematic theoretical and practical study of the features of their structure, physicochemical properties and biological activity has not been implemented.

In silico studies are now widely used in modern chemistry, as they allow one to evaluate the physico-chemical properties and pharmaceutical potential of a chemical compound based on knowledge of its structural formula [15]. The term *"in silico"* derives from the analogy with *"in vitro"* and *"in vivo"* experiments and today refers to simulations or analyses performed using computational models or digital tools, typically on a computer [16–18]. *In silico* computational tools cover a wide range of software and platforms designed to model, analyze, and predict biological, chemical, and physical processes, including techniques such as quantum chemical calculations, molecular docking and dynamics simulations, virtual screening, quantitative structure-activity relationship (QSAR) studies, machine learning, and artificial intelligence tools. *In silico* approaches are very valuable for saving time and resources by narrowing hypotheses before performing physical or biological experiments.

The aim of this study was to systematically *in silico* characterize the physicochemical and bioactive parameters of a series of 21 new synthetic analogues of natural integrastatins using quantum chemical calculations, PASS predictions, molecular docking and ADMETlab 3.0 computational tools. This will allow us to better understand the features of their structure and useful properties, as well as assess their pharmaceutical potential.

2 Experimental

2.1. Quantum-Chemical Calculations

Initially, the molecular structures of 21 studied compounds **2a-u** [1] were exported to the 2D ChemDraw editor [19], where they were assigned IUPAC names (Table S1). After that, each molecule was transformed into a 3D model using Chem3D program, its geometry was optimized according to the principle of energy minimization using the MM2 method [20] and saved in a *.mol format. Further calculations were performed using the Gaussian 16 program [21], visualization of input and output data was done using the GaussView 6.0.16 program [22].

To study the structural features and molecular properties of the studied compounds **2a–u,** DFT calculations with full geometry optimization were performed. To ensure a high level of accuracy in combination with optimal calculation time, the B3LYP exchange correlation functional and the 6-311++G(d, p) basis set [23–25] were used. A similar DFT basis set was tested by us earlier and it showed good agreement with the crystallographic data of compound **2a** [13]. Although the studied compounds are not very soluble in water, we used the macroscopic polarizable continuum model CPCM [26] to take into account the effect of the solvent (water) for better evaluation of their biologically active properties in aqueous solutions. In addition, the FREQ keyword was used to verify the truth of the obtained most stable conformation with the minimum energy and the absence of an imaginary frequency characteristic of an unstable transition state.

After optimization, analytical methods were used to construct the HOMO (Highest Occupied Molecular Orbital) and LUMO (Lowest Unoccupied Molecular Orbital) orbitals and estimate their values. Based on the calculated data, the reactivity of the studied compounds was assessed by calculating global chemical reactivity descriptors [27]. Parameters such as ionization potential (IP), electron affinity (EA), energy gap ΔE_{gap}, absolute electronegativity (χ), molecular hardness (η) and softness (σ), chemical potential (μ), index of electrophilicity (ω) and nucleophilicity (ε) were calculated using the following equations:

$$IP = -E_{HOMO}, \quad (1) \qquad \chi = (IP + EA)/2, \quad (4) \qquad \omega = \mu^2/2\eta, \quad (7)$$

$$EA = -E_{LUMO}, \quad (2) \qquad \mu = -(IP + EA)/2 = -\chi, \quad (5) \qquad \sigma = 1/2\eta, \quad (8)$$

$$\Delta E_{gap} = (E_{LUMO} - E_{HOMO}), \quad (3) \qquad \eta = (IP - EA)/2, \quad (6) \qquad \varepsilon = 1/\omega, \quad (9)$$

Also, based on the performed DFT calculations, a molecular electrostatic potential (MEP) map was constructed and analyzed to study the electrophilic and nucleophilic regions in molecules **2a-u**.

2.2. PASS Predictions

The predictive results of the PASS analysis were assessed for the test compounds **2a-u** via the PASS online platform available at http://way2drug.com/PassOnline/predict.php. This platform was developed by scientists from the Institute of Biomedical Chemistry (Moscow, Russia) and is based on a comprehensive analysis of a large data set covering chemical structures and their corresponding biological activity [28]. Predictive outputs from PASS were reported as Pa and Pi probability scores. The Pa or "activity probability" score takes values between 0 and 1 and estimates the probability that the compound under study belongs to the subclass of active compounds (resembling the molecular structures most typical of the "active" subclass of compounds in the PASS training set). The Pi score, or "inactive probability", ranges from 0 to 1 and estimates the probability that the compound under study belongs to the inactive subclass of compounds (resembling the structures of molecules most typical of the "inactive" subclass in the PASS training set). In the context of drug discovery or virtual screening, researchers may set a threshold, such as 0.5 or higher, and consider compounds with a probability score equal to or greater than this threshold as potentially active [29-30]. However, it is important to emphasize that this threshold is not rigid and can be adapted according to the specific objectives of the study, reflecting the risk tolerance and scientific objectives of researchers.

2.3. Molecular Docking

Taking into account the PASS Predictions data, a molecular docking study was performed to evaluate the antiviral inhibitory potential of test compounds **2a-u** against HIV-1 and COVID-19 virus proteins, as well as the effect on the CYP2C19 enzyme. The docking procedure was carried out using AutoDock Vina and AutoDock MGL Tools 1.5.7 [31, 32]. Protein targets were downloaded from the Protein Data Bank (https://www.rcsb.org) [33]. The human immunodeficiency virus HIV-1 reverse transcriptase protein (PDB ID: **3V81**) [34], the RNA-dependent RNA polymerase protein of the severe acute respiratory syndrome virus

SARS-CoV-2 (PDB ID: **7AAP**) [35], and the Human Microsomal Cytochrome P450 protein (PDB ID: **4GQS**) [36] as a CYP2C19 inducer were taken as targets. The preparation of the molecular structures of the proteins included the steps of removing native ligands and water molecules, protonation, and creating a binding site. The position of the binding site was determined based on PDB data, and the following grid coordinates of the receptor active site were used: ($x = 40.622$, $y = 54.348$, $z = 48.272$) for the structure of HIV-1 reverse transcriptase (PDB ID: **3V81**), ($x = 98.598$, $y = 95.084$, $z = 104.491$) for the structure of SARS-CoV-2 RNA-dependent RNA polymerase (PDB ID: **7AAP**) and ($x = -76.892$, $y = 17.61$, $z = -45.518$) for the Human Microsomal Cytochrome P450 protein (PDB ID: **4GQS**).

MM2 optimized geometry of the compounds **2a-u** was used as the initial geometry of the ligands. Based on the docking results, a comparative analysis of the binding affinity and intermolecular interactions between the studied compounds **2a-u** and the proteins was performed. The study of non-covalent interactions between proteins and ligands was performed using the BIOVIA Discovery Studio Visualizer 2017 program [37].

2.4. ADMET Properties

ADMET (Absorption, Distribution, Metabolism, Excretion, and Toxicity) properties of chemical compounds are key pharmacokinetic and pharmacodynamic characteristics of drugs that influence their therapeutic potential. These properties play an important role in the drug development and safety evaluation process as they allow one to study how potential drug candidates will behave in the human body, assessing their absorption into the bloodstream, distribution to target tissues, metabolism by enzymes, elimination from the body and any potential toxicity issues [38, 39]. The ADMET criteria are based on the understanding that compounds that do not meet established thresholds may exhibit problems with membrane permeability, oral absorption, and pharmacokinetic characteristics. Thus, ADMET studies allow testing of the interaction of a compound with biological systems and guide decision-making in the drug development process.

ADMET profiles of the compounds **2a, 2r** and **2u** were assessed using the ADMETlab 3.0 comprehensive online tool (https://admetlab3.scbdd.com/) [40]. The drug-likeness of these compounds was assessed using Lipinski's rule of 5 [41], which predicts that molecules exceeding thresholds of five hydrogen bond donors, ten hydrogen bond acceptors, a molecular weight greater than 500 Da, and an estimated LogP greater than five are likely to exhibit poor absorption or penetration [42]. As a result, compounds that do not meet these requirements are generally considered unsuitable for oral bioavailability as pharmaceuticals [43].

3 Results and Discussion

3.1. Quantum — Chemical Calculations

The geometry optimization procedure of the studied compounds **2a-u** and evaluation of their calculated quantum-chemical parameters was carried out by the DFT B3LYP 6-311++G(d, p) CPCM (solvent — water) method using the Gaussian 16 program.

Quantum chemical geometry optimization procedure involves the automatic search for the most stable and energetically favorable conformation of a molecule by minimizing its potential energy. The resulting geometry of the molecule corresponds to its most energetically stable stationary state, which plays an important role in determining its physicochemical and biological properties, as well as its reactivity. Figure S2 shows the obtained optimized geometries of the studied molecules **2a-u,** which have a complex structure due to the presence of an oxocine ring in the center of the molecule, conjugated on one side with a benzene ring, and on the other side with a heterocyclic nitrogen-containing pyridine ring. The inclusion of various substituents ($-OH$, $-Br$, $-NO_2$, $-OCH_3$, $-CHO$, $-CH_2CHCH_2$, $-C_6H_4-$) into various positions of the side benzene ring allows modeling the physicochemical and biologically active properties of the molecules under study. The non-planar structure of the studied compounds is due, first of all, to the chair-shaped structure of the central epoxybenzo[7,8]oxocine fragment. The main "kink" of the molecules under study occurs in the oxocinic ring, which, due to its structural features, orients the two parts of the molecule almost perpendicular to each other (Fig. 3).

a) front view[*]

b) side view[*]
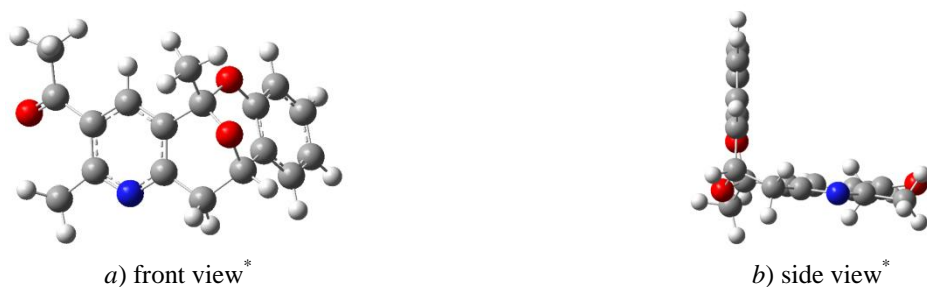
Note: [*]Gray spheres represent carbon atoms (C), white spheres represent hydrogen atoms (H), red spheres represent oxygen atoms (O), blue spheres represent nitrogen atoms (N).

Figure 3. Optimized geometry of **2a** molecule

The analysis of the frontier orbitals of the studied molecules was performed (Table S3, Figure 4) in order to assess global chemical reactivity descriptors of compounds **2a-u**.

HOMO

LUMO

2a

2b
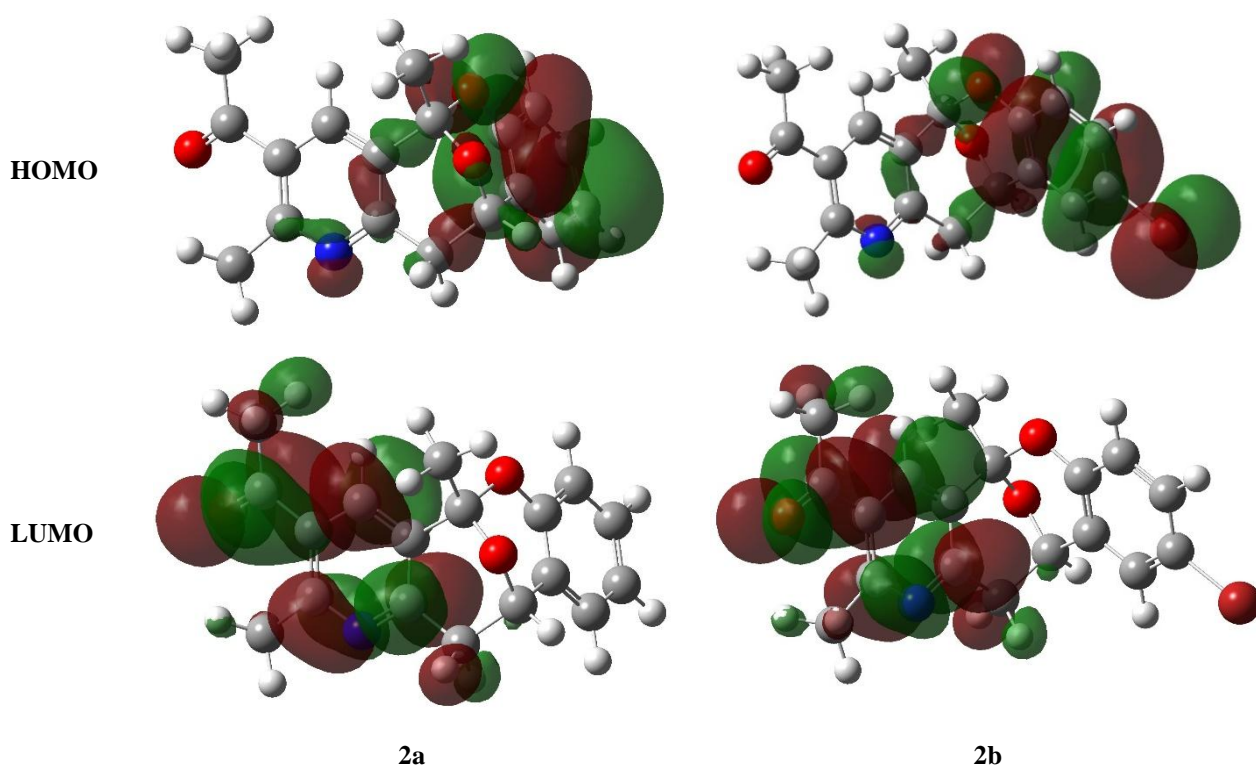
Figure 4. HOMO-LUMO diagrams for **2a** and **2b** molecules

As can be seen from the diagrams in Figure 4, the HOMO and LUMO orbitals are separated in space and localized in different parts of the molecules **2a-u.** The HOMO is mainly distributed over the epoxybenzo[7,8]oxocine fragment and the side substituent of the benzene ring, whereas the LUMO is delocalized over the acetylpyridine fragment. This separation in the space of HOMO and LUMO orbitals indicates the separation of nucleophilic and electrophilic centers of the studied molecules **2a-u.**

Based on the characteristics of HOMO and LUMO orbitals, global chemical reactivity descriptors were estimated, such as: ionization potential (IP), electron affinity (EA), energy gap ΔE_{gap}, molecular hardness (η) and softness (σ), absolute electronegativity (χ) and chemical potential (μ), electrophilicity (ω) and nucleophilicity (ε) indexes (Table 1).

Global chemical reactivity descriptors of the studied compounds

Com-pound	Parameter								
	IP	EA	ΔE_{gap}	η	σ	χ	μ	ω	ε
2a	6.533185	2.138272	4.394913214	2.197457	0.227536	4.335728	–4.33573	4.277341	0.23379
2b	6.499987	2.180994	4.318993408	2.159497	0.231535	4.34049	–4.34049	4.362094	0.229248
2c	7.06925	3.003866	4.06538316	2.032692	0.245979	5.036558	–5.03656	6.239736	0.160263
2d	6.066782	2.158408	3.908373382	1.954187	0.255861	4.112595	–4.11259	4.327488	0.231081
2e	5.988957	2.138	3.850957328	1.925479	0.259676	4.063478	–4.06348	4.287728	0.233224
2f	6.835504	2.201402	4.63410142	2.317051	0.215792	4.518453	–4.51845	4.405691	0.226979
2g	6.328555	2.135279	4.19327674	2.096638	0.238477	4.231917	–4.23192	4.270913	0.234142
2h	6.362842	2.146163	4.216678544	2.108339	0.237153	4.254502	–4.2545	4.292666	0.232955
2i	6.956594	2.860734	4.095859928	2.04793	0.244149	4.908664	–4.90866	5.882766	0.169988
2j	6.041747	2.135006	3.906740698	1.95337	0.255968	4.088377	–4.08838	4.278458	0.233729
2k	6.142974	2.155959	3.987014328	1.993507	0.250814	4.149466	–4.14947	4.318538	0.23156
2l	6.612642	2.178	4.434641858	2.217321	0.225497	4.395321	–4.39532	4.35635	0.22955
2m	6.919859	2.272152	4.64770712	2.323854	0.21516	4.596005	–4.59601	4.544879	0.220028
2n	7.106257	3.108902	3.99735466	1.998677	0.250165	5.10758	–5.10758	6.526159	0.153229
2o	6.451823	2.971485	3.48033806	1.740169	0.287328	4.711654	–4.71165	6.378599	0.156774
2p	7.210205	3.067813	4.142391422	2.071196	0.241406	5.139009	–5.13901	6.375403	0.156853
2q	6.904076	3.077881	3.826194954	1.913097	0.261356	4.990979	–4.99098	6.510351	0.153602
2r	7.309254	3.244415	4.064838932	2.032419	0.246012	5.276835	–5.27683	6.850206	0.145981
2s	6.511416	2.169293	4.342123098	2.171062	0.230302	4.340354	–4.34035	4.338586	0.23049
2t	7.071699	2.944001	4.127697266	2.063849	0.242266	5.00785	–5.00785	6.075679	0.164591
2u	6.136987	2.144258	3.992728722	1.996364	0.250455	4.140623	–4.14062	4.293995	0.232883

Note: *IP*—ionization potential (eV); *EA* — electron affinity (eV); ΔE_{gap} — frontier molecular orbitals energy gap (eV); η — chemical hardness (eV); σ — chemical softness (eV^{-1}); χ — electronegativity (eV); μ — chemical potential (eV); ω — electrophilicity (eV); ε — nucleophilicity (eV^{-1}).

The global descriptors presented in Table 1 define the chemical reactivity of molecules **2a-u** as a whole. Thus, the ionization potential IP characterizes the ability of a molecule to give up an electron, and the lower it is, the easier the molecule gives up an electron, exhibiting reducing properties. All the studied molecules **2a-u** have a fairly high ionization potential, from 5.9 to 7.1 eV, which indicates their low reducing properties. Electron affinity characterizes the oxidative properties of molecules, and the higher it is, the higher the oxidation potential of the compound. The electron affinity EA varies from 2.1 to 3.2 eV for the studied compounds **2a-u**, which indicates their low oxidizing ability. Large energy gap ΔE_{gap} between HOMO and LUMO orbitals characterizes the high chemical stability of the compound. The energy gap ΔE_{gap} ranges from 3.8 to 4.6 eV for **2a-u** molecules, which indicates their chemical stability. The chemical hardness η of a molecule is determined by its resistance to deformation under the influence of an external electric field and the effect of chemical reactions. An increase in molecular hardness is associated with an increase in stability and a decrease in reactivity. A hardness compound has a large HOMO − LUMO gap, so the molecule with the smallest HOMO gap and LUMO has the highest reactivity. A high value of chemical softness σ indicates high polarizability of the molecule. A chemical compound is considered hard if the energy gap between HOMO and LUMO exceeds 1 eV. From the data presented in Table 3 it is evident that the hardness of the studied molecules **2a-u** varies from 1.7 to 2.3 eV, which, together with a fairly large energy gap from 3.8 to 4.6 eV indicates the hardness nature of the compounds. At the same time, the low softness value of about 0.2 eV indicates the average hardness of the compounds **2a-u.** Absolute electronegativity χ is defined by Mulliken as the half-sum of the first ionization potential and the electron affinity χ = 0.5(*IP* + *EA*). The electronegativity for molecules **2a-u** lies in the range of 4.0–5.1 eV. The electron chemical potential is electronegativity with the opposite sign, for the studied compounds **2a-u** the chemical potential **μ** has negative values in the range from –4.1 to –5.2 eV. The value of the electrophilicity index **ω** lies in the range of 4.1–6.8 eV, which indicates the tendency of the molecules **2a-u** to accept electrons. This is also confirmed by the low values of the nucleophilicity index *ε* in the range of 0.1–0.2 eV^{-1}.

Molecular electrostatic potential (MEP) analysis was applied to investigate the electrophilic and nucleophilic sites in the molecules **2a-u** (Figure S4). On the MEP surface, the most favorable nucleophilic

center, as expected, is located on the carbonyl oxygen atom, while other negative electrostatic potential sites are located on the remaining oxygen and nitrogen atoms. The hydrogen atom of pyridine is one of the most electrophilic regions of **2a-u** (Fig. 5).
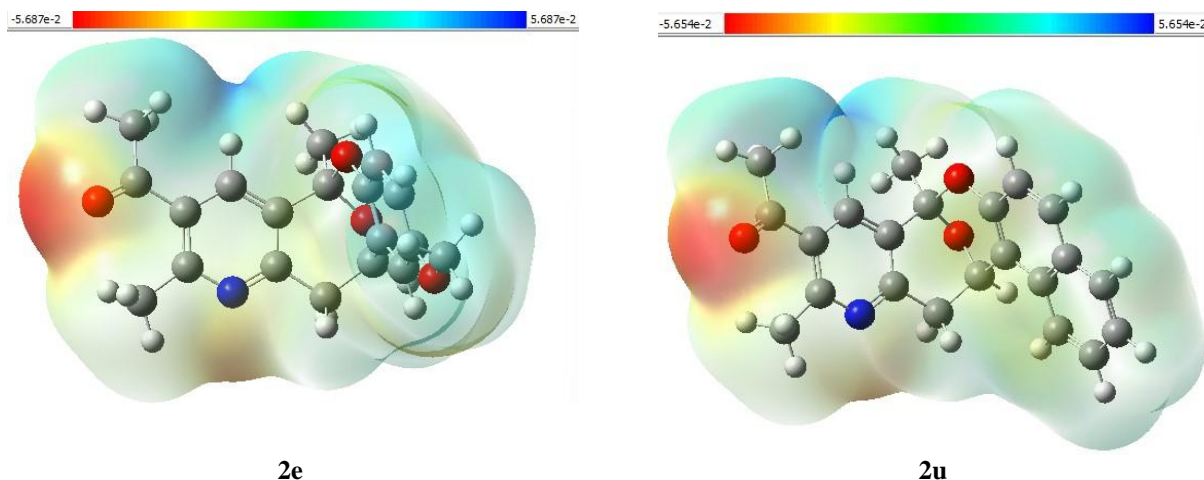

| **2e** | **2u** |

Figure 5 Map of electrostatic potentials for **7e** and **7u** molecules

Thus, the applied complex quantum-chemical approach contributed to a deeper understanding of the electronic structure and molecular properties of the studied compounds **2a-u**, as well as to the identification of their reaction centers and the assessment of the chemical potential for subsequent *in silico* studies of biological activity.

3.2. PASS (Prediction of Activity Spectra for Substances) Predictions

The PASS Online Internet resource (https://www.way2drug.com/passonline/) was used to assess the potential biological activity of the studied compounds **2a-u.** This online tool allows predicting more than 4000 types of biological activity in the form of Pa (the probability of being active) and Pi (the probability of being inactive) values based on the structural formula of a chemical compounds. Thus, a high probability of antiviral and antibacterial activity of the studied compounds **2a-u** was established, and it was also shown that all the studied molecules can be CYP2C19 inducers and proton pump inhibitors, and most are histidine kinase inhibitors. The corresponding Pa and Pi values for the studied compounds **2a-u** are presented in Table 2.

T a b l e   2

PASS prediction data

Compound	Antiviral		CYP2C19 inducer		General pump inhibitor		Histidine kinase inhibitor		Antibacterial	
	Pa	Pi	Pa	Pi	Pa	Pi	Pa	Pi	Pa	Pi
2a	0.543	0,013	0,610	0.005	0.563	0.035	0.528	0.024	0.278	0.068
2b	0.492	0.027	0.555	0,008	0.410	0.127	0.425	0.045	0.293	0.063
2c	0.483	0.031	0.547	0,008	0.540	0.043	0.411	0.049	0.322	0.052
2d	0,520	0,018	0.564	0,007	0.616	0,021	0.658	0,011	0.328	0,050
2e	0.529	0.016	0.560	0,008	0.594	0.026	0.469	0.034	0.251	0.082
2f	0.499	0.025	0,570	0,007	0.435	0.103	0.489	0,030	0.376	0.036
2g	0.531	0,016	0.575	0,007	0.592	0.027	0.684	0,009	0.344	0.045
2h	0.491	0.028	0.540	0,009	0.441	0.099	0.559	0.020	0.378	0.036
2i	0.482	0.031	0.532	0,009	0.514	0.053	0.545	0.022	0.399	0,030
2j	0.492	0.027	0.528	0,009	0.477	0.073	0.260	0.139	0.337	0.047
2k	0.463	0,041	0.535	0,009	0.405	0.132	0.299	0.103	0.227	0.097
2l	0.457	0.044	0.555	0,008	–	–	0.312	0.094	0.347	0.044
2m	0.427	0.065	0.541	0,009	–	–	0.338	0.078	0.387	0.033
2n	0.417	0.074	0.521	0,010	0.344	0.207	0.270	0.127	0.307	0.057
2o	0.454	0.046	0.527	0,010	0.475	0.074	0.288	0,111	0.205	0.113
2p	0.417	0.074	0.533	0,009	–	–	0.327	0.085	0.339	0.046

C o n t i n u a t i o n   o f   T a b l e   2

Compound	Antiviral		CYP2C19 inducer		General pump inhibitor		Histidine kinase inhibitor		Antibacterial	
	Pa	Pi	Pa	Pi	Pa	Pi	Pa	Pi	Pa	Pi
2q	0.417	0.074	0.521	0,010	–	–	0.270	0.127	0.231	0.094
2r	0.447	0,050	0.547	0,008	0.410	0.127	0.301	0.102	0.242	0.087
2s	0.452	0.047	0,540	0,009	0.353	0.195	0.416	0.047	0.346	0.044
2t	0.416	0.075	0.508	0,011	0.372	0,170	0.368	0.064	0.278	0.068
2u	0.523	0,018	0.593	0.006	0.598	0.025	0.532	0.024	0.249	0.084

Note: Pa is the probability of being active; Pi is the probability of being inactive.

The data presented in Table 2 show that the highest Pa values of compound **2a-u** were in the region of antiviral activity (Pa~0.416–0.523). Antiviral activity refers to the ability of a substance or compound to inhibit the reproduction of viruses or destroy viral particles. Today there are many viruses that are dangerous to humans, including the human immunodeficiency virus (HIV-1), which destroys the immune system and makes a person vulnerable to various infections and diseases, and the coronavirus, which causes COVID-19 and can lead to serious complications and death, especially in people predisposed to this disease. These HIV-1 and COVID-19 viruses pose a significant threat to human health and require special attention and precautions to prevent their spread.

Also, compounds **2a-u** have demonstrated relatively high Pa values as CYP2C19 inducers (Pa~0.508–0.610). CYP2C19 inducers are substances that increase the activity of the CYP2C19 enzyme, which belongs to the cytochrome P4501 family. This enzyme plays an important role in the metabolism of many drugs, including some proton pump inhibitors, antiepileptic drugs, and anticoagulants. Examples of drugs that induce CYP2C19 include: rifampin, an antibiotic used to treat tuberculosis; phenobarbital, an anticonvulsant used to treat various types of epilepsy; carbamazepine, an anticonvulsant used to treat various types of epilepsy and pain associated with trigeminal neuralgia; primidone, an anticonvulsant used to treat generalized, psychomotor, and focal epileptic seizures. Induction of CYP2C19 may affect drug metabolism, which may require dose adjustment or selection of alternative drugs.

Most compounds **2a-u** with a probability of Pa~0.344–0.598 can exhibit biological activity as Proton Pump Inhibitors (PPIs), a class of drugs that reduce the production of gastric acid. They act by irreversibly blocking the enzyme H^+/K^+-ATPase (Hydrogen/Potassium ATPase), which controls acid production in the parietal cells of the stomach wall. This enzyme is also known as the proton pump. PNIs are widely used to treat conditions such as: chronic gastroesophageal reflux disease (CGER), duodenal and gastric ulcers, erosive esophagitis, malignant necrotizing pancreatitis, Zollinger-Ellison syndrome. Examples of PNI drugs include omeprazole (Prolon), lansoprazole (Prevacard), esomeprazole (Nexium) and pantoprazole (Protonix).

All studied compounds **2a-u** may also exhibit biological activity with Pa~0.270–0.684 as histidine kinase inhibitors (HKIs), a class of drugs that block the activity of histidine kinases. Histidine kinases are enzymes that play an important role in cell signaling, especially in bacteria. They are involved in so-called two-component signaling systems that help bacteria adapt to different environmental conditions. HKIs can be used to develop new antibacterial drugs, as they can block multiple regulatory networks associated with pathogenicity and antibiotic resistance. These inhibitors may be useful in the fight against microbial infections, especially in conditions where bacteria are becoming resistant to traditional antibiotics.

Compounds **2a-u** are predicted to also exhibit weak antibacterial activity with Pa~0.205–0.399, which refers to the ability of a substance to inhibit the growth of or kill bacteria. Substances with antibacterial activity are used to treat and prevent bacterial infections. Some of the most common and dangerous bacterial infections in humans are: tuberculosis — caused by the bacterium *Mycobacterium tuberculosis (Koch's bacillus)* and can affect the lungs and other organs; anthrax — caused by the gram-positive bacterium *Bacillus anthracis* and can lead to serious infections of the skin, lungs, and intestines; salmonellosis — caused by the bacterium *Salmonella* and is often associated with contaminated food; sepsis — a serious blood infection caused by various bacteria, such as *Staphylococcus aureus* and *Escherichia coli*; meningitis — an inflammation of the meninges caused by bacteria such as *Neisseria meningitidis* and *Streptococcus pneumoniae;* cholerae — caused by the bacterium *Vibrio cholerae* and results in severe dehydration and diarrhea; pneumonia — inflammation of the lungs caused by various bacteria such as *Streptococcus pneumoniae* and *Mycoplasma pneumoniae*; gonorrhea — a sexually transmitted infection caused by the bacterium *Neisseria gonorrhoeae*; syphilis — a chronic disease caused by the bacterium *Treponema pallidum*. These infections

can be very serious and require treatment with antibacterial drugs. Antibacterial substances can work in a variety of ways, including inhibiting bacterial cell wall synthesis, suppressing protein synthesis, disrupting the cell membrane, or inhibiting DNA synthesis. Some plants and natural compounds, such as honey and garlic extracts, also have antibacterial activity. Antibacterial substances are widely used to treat infections caused by bacteria, such as pneumonia, urinary tract and skin infections. Antibacterial activity plays an important role in medicine and helps prevent and treat infectious diseases.

In summary, the evaluation of the potential biological activity of the studied compounds **2a-u** using the PASS Online resource revealed their antiviral and inhibitory potential as CYP2C19 inducers. These types of biological activities of compounds **2a-u** were further investigated using molecular docking method. Antiviral activity was assessed against such relevant diseases as human immunodeficiency virus (HIV-1) and COVID-19, caused by infection with severe acute respiratory syndrome coronavirus 2, also called SARS-CoV-2.

3.3. Molecular Docking

The molecular docking method using the AutoDock Vina program was applied for a more thorough assessment of the antiviral and inhibitory potential as CYP2C19 inducers of the studied molecules **2a-u**. The protein structure of human immunodeficiency virus HIV-1 reverse transcriptase protein (PDB ID: **3V81**), SARS-CoV-2 RNA-dependent RNA polymerase (PDB ID: **7AAP**) and the Human Microsomal Cytochrome P450 protein (PDB ID: **4GQS**) [36] as a CYP2C19 inducer were chosen as the target proteins. Well-known drugs were taken as reference drugs. Nevirapine was taken as an antiretroviral drug used to treat and prevent HIV-1 infection, Favipiravir was taken as an antiviral drug that inhibits RNA-dependent RNA polymerase of viruses (including COVID-19), preventing their replication, and Rifampin was taken as an antibacterial drug — CYP2C19 inducer used to treat tuberculosis and other bacterial infections. Table 3 presents the binding affinity of the studied compounds **2a-u** with target proteins obtained as a result of molecular docking procedure.

T a b l e 3

Results of Molecular Docking of 2a-u compounds with targets proteins

No.	Compound	Binding affinity, kcal/mol		
		HIV-1 protein (3V81)	SARS-CoV-2 protein (7AAP)	CYP2C19 inducer (4GQS)
Reference drug				
1	Nevirapine	**−9.0**		
2	Favipiravir		**−7.0**	
3	Rifampin			**−7.8**
Ligand				
1	**2a**	−9.7	−7.3	−8.9
2	**2b**	−9.0	−7.3	−7.1
3	**2c**	−9.8	−7.3	−7.9
4	**2d**	−9.3	−7.6	−9.3
5	**2e**	−8.9	−7.7	−6.9
6	**7f**	−9.3	−7.7	−8.5
7	**7g**	−9.1	−7.6	−7.4
8	**2h**	−9.0	−7.6	−7.1
9	**2i**	−9.6	−7.6	−7.7
10	**2j**	−8.9	−7.9	−6.9
11	**2k**	−8.8	−7.6	−7.1
12	**2l**	−9.0	−7.3	−7.3
13	**2m**	−9.0	−7.6	−7.6
14	**2n**	−9.0	−7.8	−7.4
15	**2o**	−9.0	−7.1	−6.8
16	**2p**	−9.1	−7.7	−7.0
17	**2q**	−9.1	−7.5	−6.8
18	**2r**	−9.2	−7.8	**−9.4**
19	**2s**	−9.2	−6.7	−7.2
20	**2t**	−9.2	−7.7	−7.3
21	**2u**	**−10.2**	**−9.3**	−8.0

As can be seen in Table 3, all tested compounds **2a-u** demonstrated high binding affinity, even compared to the reference drugs. Compound **2u** showed the highest antiviral potential against the HIV-1 virus (Binding Affinity = –10.2 kcal/mol) and against the SARS-CoV-2 virus (Binding Affinity = –9.3 kcal/mol). The binding affinity of **2u** compound to 3V81 and 7AAP receptors is higher than that of the reference drugs Nevirapine (Binding affinity = –9.0 kcal/mol) and Favipiravir (Binding Affinity = –7.0 kcal/mol), respectively. Ligand **2r** was found to be the best CYP2C19 inducer with a binding affinity of –9.4 kcal/mol compared to –7.8 kcal/mol for the reference drug Rifampicin.

Intermolecular interactions predominantly determine the binding efficiency of the top compounds **2u** and **2r** to the **3V81**, **7AAP** and **4GQS** receptors, so their analysis was performed (Figures 6–8, Table 4).
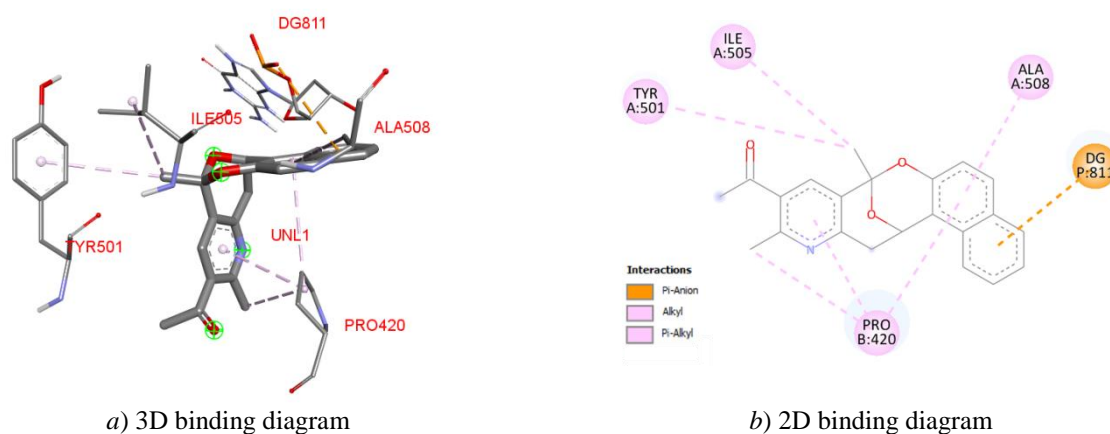

a) 3D binding diagram   *b*) 2D binding diagram

Figure 6. Visualization of **3V81** protein — 2**u** ligand interactions

a) 3D binding diagram   *b*) 2D binding diagram

Figure 7. Visualization of **7AAP** protein — 2**u** ligand interactions

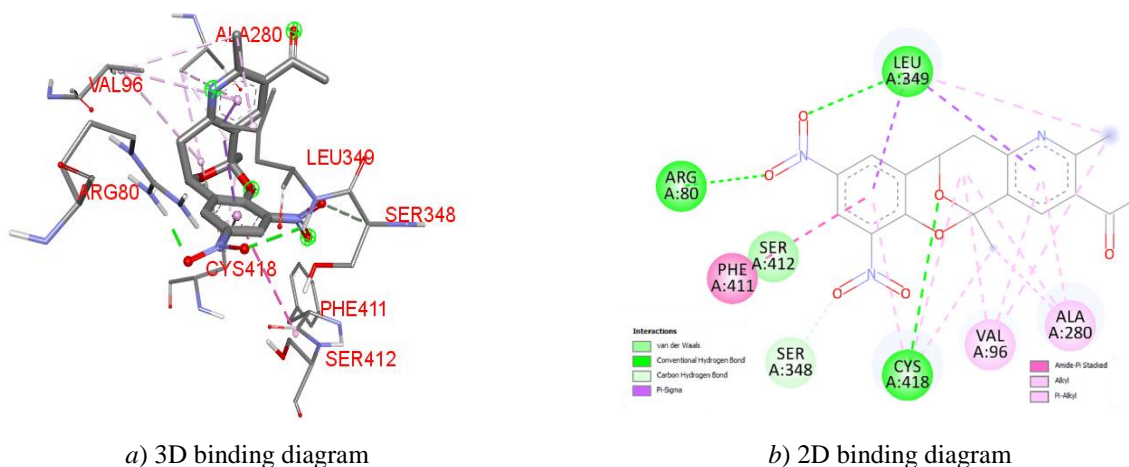*a*) 3D binding diagram   *b*) 2D binding diagram

Figure 8. Visualization of **4GQS** protein– 2**r** ligand interactions

Table 4

Protein-Ligand Interactions

Ligand	Protein	Conventional Hydrogen Bond	Pi-Anion	Pi-Pi T-shaped	Alkyl	Pi-Alkyl
2u	3V81	–	DG811	–	TYR501	ILE505, PRO420, ALA508
2u	7AAP	ASN39	LYS50, ILE37	PHE35	–	ASP221
2r	4GQS	LEU359, CYS418, ARG80	SER348	SER412	VAL96, ALA280	PHE411

As can be seen in Figures 6–8 and Table 4, the most common types of intermolecular protein-ligand interactions are hydrogen and π-bonds. In particular, the ligand **2u** in complex with the protein **3V81** has demonstrated a distinct Pi-Anion interaction with DG811, which was facilitated by the conjugated benzene group on the ligand, indicating a unique binding orientation. Ligand **2u** also demonstrated Pi-Alkyl interactions with ILE505, PRO420, and ALA508 amino acids, but through different functional groups, suggesting alternative binding modes that may affect its potency and specificity (Table S5). Ligand **2u** in the complex with the second viral protein 7AAP showed hydrogen bonding with ASN39, as well as Pi-Anion binding with LYS50 and ILE37, Pi-Pi T-shaped binding with PHE35 and Pi-alkyl binding with ASP221 amino acids (Table S6).

Also ligand **2r** in the complex with the CYP2C19 inducer protein **4GQS** showed formation of three hydrogen bonds with LEU359, CYS418 and ARG80 amino acids, as well as Pi-Anion bonding with SER348, Pi-Pi T-shaped binding to SER412, Pi-Alkyl binding to PHE411, and Alkyl binding to VAL96 and ALA280 amino acids (Table S7). In general, hydrogen bonds and pi-bonds predominate in intermolecular interactions of the top **2r** and **2u** compounds with the target proteins, which directly affect the stability and specificity of the resulting ligand-protein complexes, influencing the overall docking score and potential biological activity of the compounds.

Thus, the molecular docking study showed the high antiviral potential of all 21 studied compounds against the HIV-1 and SARS-CoV-2 viruses. Ligand **2u** showed the best binding to both viral proteins. Human immunodeficiency virus HIV-1 reverse transcriptase protein (PDB ID: **3V81**) and protein of the RNA-dependent RNA polymerase of the SARS-CoV-2 (PDB ID: **7AAP**) can serve as a likely biological target for the compounds **2a-u**. The inhibitory potential of compounds **2a-u** as CYP2C19 inducers was also assessed using molecular docking procedure, and ligand **7r** showing the highest binding affinity with the **4GQS** protein.

3.4. ADMET Properties

At the final stage of the study, three representatives of the studied compounds — compounds **2a, 2r** and **2u** — were subjected to *in silico* evaluation of ADMET properties using the ADMETlab 3.0 online portal. First of all, the physicochemical properties of the compounds were estimated, such as molecular weight (MW), number of hydrogen bond donors (nHA) and acceptors (nHD), number of freely rotating bonds (nRot), number of rings (nRing) and heteroatoms (nHet), topological polar surface area (TPSA), logarithm of water solubility (log$S$), logarithm of *n*-octanol/water partition coefficients at pH = 7.4 (log$P$), logarithm of *n*-octanol/water partition coefficient (log$D$), as well as their compliance with the Lipinski's Rule of Five (Table 5, Figure 9).

Table 5

Physicochemical properties of the studied compounds and Lipinski's Rule

Compound	MW, Da	nHA	nHD	nRot	nRing	MaxRing	nHet	nRig	TPSA, Å²	log$S$	log$P$	log$D$	Lipinski's Rule
2a	295.12	4	0	1	4	16	4	21	48.42	–3.147	2.347	2.395	Yes
2r	385.09	10	0	3	4	16	10	23	134.7	–4.308	2.0	2.363	Yes
2u	345.14	4	0	1	5	20	4	26	48.42	–4.552	3.506	3.17	Yes

Note: MW— molecular weight of the molecule (Optimal: <500 Da), nHA — Number of hydrogen bond acceptors (Optimal:0~12), nHD — Number of hydrogen bond donors (Optimal:0~7), nRot — Number of rotatable bonds (Optimal: 0~11), nRing — Number of rings (Optimal:0~6), MaxRing — Number of atoms in the biggest ring (Optimal: 0~18), nHet — Number of heteroatoms (Optimal: 1~15), nRig — Number of rigid bonds (Optimal: 0~30), TPSA — Topological Polar Surface Area (Optimal: 0~140 Å²), log$S$ — logarithm of aqueous solubility value, log$P$ — logarithm of the *n*-octanol/water distribution coefficients at pH = 7.4, log$D$ — logarithm of the *n*-octanol/water distribution coefficient, Lipinski Rule — MW ≤ 500; log$P$ ≤ 5; nHA ≤10; nHD ≤ 5. If two properties are out of range, a poor absorption or permeability is possible, one is acceptable.
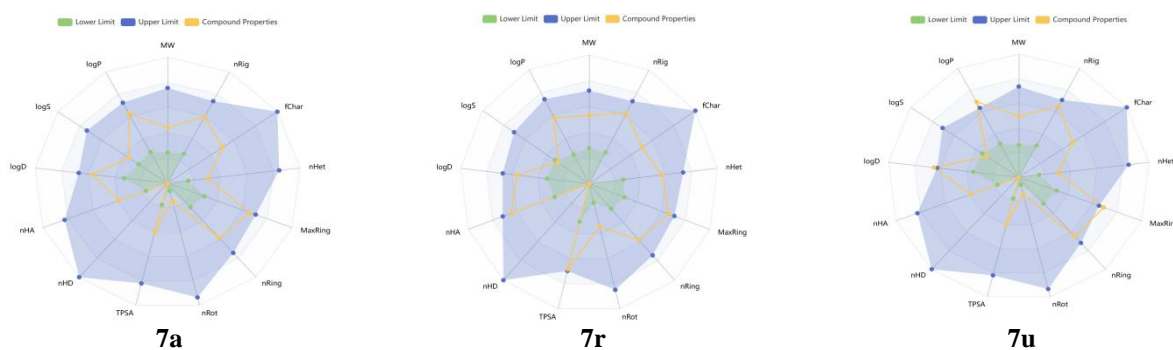
Figure 9. Radar view of the physicochemical properties of the studied compounds **7a, 7r** and **7u**

As can be seen in Table 5, all the studied compounds with MM = 295.12–385.09 Da fall within the acceptable molecular weight range for drug-like molecules. Higher molecular weights can sometimes indicate complexity of synthesis and potential cell permeability problems, but all values here are within the acceptable range of <500 Da. The number of hydrogen bond acceptors nHA varies from 4 to 10, indicating the presence in **2a, 2r** and **2u** molecules of oxygen and nitrogen atoms, which have unpaired electrons and can form hydrogen bonds with other molecules. At the same time, the **2a, 2r** and **2u** molecules do not contain atoms that can donate hydrogen bonds (nHD = 0). These are usually hydrogen atoms bonded to oxygen or nitrogen atoms that can form hydrogen bonds with hydrogen bond acceptors. Both of these properties are important in chemistry and pharmaceuticals because they affect the interaction of molecules with biological targets and their solubility in water.

The number of rotatable bonds (nRot) for all compounds is moderate (from 1 to 3), indicating some flexibility without excessive molecular complexity that could hinder oral bioavailability. The number of ring structures (nRing) in the **2a, 2r** and **2u** molecules varies from 4 to 5, which corresponds to the optimal range (from 0 to 6) ring structures for pharmaceutical compounds. These rings can be both aromatic and non-aromatic. The number of atoms in the largest ring MaxRing is 16 for **7a** and **7r** molecules, and 20 for **2u**. This property shows the size of the largest ring structure in the molecule, which is important for assessing its stability and interaction with biological targets.

Heteroatoms play an important role in the chemical and biological properties of molecules, as they can participate in hydrogen bonds, affect the polarity and reactivity of compounds. The optimal range for pharmaceutical compounds is usually from 1 to 15 heteroatoms. The number of heteroatoms (nHet) in the studied compounds **2a, 2r** and **2u** varies from 4 to 10, which is within the recommended range.

The number of rigid bonds (nRig) in the studied molecules ranged from 21 to 26, which is within the optimal range of 0 to 30 rigid bonds for pharmaceutical compounds. Rigid bonds cannot rotate due to their structure, but their presence is important because they affect the three-dimensional structure of the molecule and its interaction with biological targets. The more rigid bonds reduce the flexibility of the molecule, which can be both an advantage and a disadvantage depending on the context.

The optimal range of TPSA (Topological Polar Surface Area) for pharmaceutical compounds is usually from 0 to 140 Å². The total area of all polar surfaces of a molecule is calculated based on its topological structure and for the studied compounds it was 48.42 Å² for molecules **2a** and **2u,** and 134.7 Å² for **2r** molecules. In this range, molecules have good absorption and penetration through biological membranes, which is important for their bioavailability.

The correct ratio of solubility coefficients in water and non-polar media is important for molecules that are potential medicinal substances, since it affects the behavior of the substance in various biological environments. Thus, within the framework of *in silico* evaluation of ADMET properties of the studied compounds **2a, 2r** and **2u,** the following parameters were considered: log$S$ — the logarithm of the solubility of a substance in water (compounds in the range up to 0.5 can be considered soluble), log$P$ — the logarithm of the distribution coefficient of a substance between *n*-octanol and water at pH 7.4 (compounds in the range from 0 to 3 can be considered suitable), and log$D$ — logarithm of the partition coefficient of a substance between *n*-octanol and water at a certain pH (compounds in the range from 1 to 3 can be considered suitable). As can be seen in Table 5 that substances **2a, 2r** and **2u** have negative log$S$ values, which indicates their poor solubility in water. At the same time, log$P$ values in the range from 2.0 to 3.506 indicates their high lipophilicity, which is also confirmed by high positive log D values in the range from 2.363 to 3.17.

Overall, all three studied compounds comply with Lipinski's Rule of Five, which states that they have a molecular weight of less than 500 Da, a log P value less than 5, a number of hydrogen bond donors (nHD) no more than 5, a number of hydrogen bond acceptors (nHA) no more than 10, and a topological polar surface area (TPSA) less than 140 Å².

In conclusion ADMET properties of the compounds **2a, 2r** and **2u** were *in silico* assessed (Table 6).

Table 6

***In silico* ADMET properties of the studied compounds**

Compound	Absorption		Distribution		Metabolism				Excretion		Toxicity	
	Caco2 permeability	MDCK permeability	BBB Penetration	PPB (%)	CYP2C19 inhibitor	CYP2C19 substrate	CYP2C9 inhibitor	CYP2C9 substrate	CL_{plasma}	$T_{1/2}$	Hematotoxicity	RPMI-8226 Immunotoxicity
2a	–4.778	–4.62	1.0	96.383	0.847	0.039	0.674	0.009	7.302	0.862	0.534	0.223
2r	–4.809	–4.396	0.837	98.564	0.998	0.989	1.0	0.0	4.682	0.894	0.78	0.227
2u	–4.746	–4.61	0.999	97.458	0.999	0.486	0.545	0.0	5.388	0.588	0.409	0.21

Note: Caco2 Permeability (Optimal: higher than –5.15 Log unit); BBB Penetration — Blood-Brain Barrier Penetration (Category 1: BBB+; Category 0: BBB-); PPB — Plasma Protein Binding (Optimal: < 90 %); CYP2CX inhibitor — Category 1: Inhibitor; Category 0: Non-inhibitor, CYP2CX substrate — Category 1: Substrate; Category 0: Non-substrate, CLplasma — unit of predicted CL_{plasma} penetration is ml/min/kg: >15 ml/min/kg: high clearance; 5–15 ml/min/kg: moderate clearance; < 5 ml/min/kg: low clearance, $T_{1/2}$ — unit of predicted $T_{1/2}$ is hours: ultra-short half-life drugs: 1/2 < 1 hour; short half-life drugs: $T_{1/2}$ between 1–4 hours; intermediate short half-life drugs: $T_{1/2}$ between 4–8 hours; long half-life drugs: $T_{1/2} > 8$ hours, Hematotoxicity — Category 0: non-hematotoxicity (-); Category 1: hematotoxicity (+), RPMI-8226 Immunotoxicity — Category 0: non-cytotoxicity (-); Category 1: cytotoxicity (+).

As can be seen in Table 6, the studied compounds **2a, 2r** and **2u** are characterized by good Caco2 permeability (> –5.15 Log unit), which indicates a potentially high oral efficacy of the drug. The MDCK permeability assessment also predicts good absorption of the studied compounds in the human gastrointestinal tract. BBB (blood-brain barrier) penetration is the penetration of drugs acting on the central nervous system through the blood-brain barrier. These values were in the range of 0.837–1.0 for the studied compounds **2a, 2r** and **2u**, which indicates their low potential for the blood-brain barrier penetrating.

The CYP2C19 inhibitor, CYP2C19 substrate, CYP2C9 inhibitor and CYP2C9 substrate values were analyzed to evaluate the metabolic potential of the compounds **2a, 2r** and **2u**, which is important for understanding drug interactions and their side effects. The analysis showed that compounds **2a, 2r** and **2u** have the potential to inhibit the CYP2C19 enzyme, slowing its ability to catalytically metabolize other compounds.

The CL_{plasma} and $T_{1/2}$ parameters were analyzed to assess the excretion potential of the **2a, 2r** and **2u** compounds. CL_{plasma} indicator characterizes the rate of removal of a substance from blood plasma and $T_{1/2}$ parameter characterizes the time during which the concentration of a substance in the body decreases by half. As can be seen in Table 6, compounds **2a, 2r** and **2u** have a moderate clearance of 4.682–7.302 in CL_{plasma}, i.e. they are excreted from the body with an average $T_{1/2}$ rate of about 1 hour.

The toxicity of the studied compounds was assessed using hematotoxicity and immunotoxicity parameters. These parameters for the compounds **2a, 2r** and **2u** fell within the ranges of 0.409–0.78 and 0.21–0.227, respectively, suggesting a promising safety profile for therapeutic use.

In summary, comprehensive assessment of ADMET properties of the compounds **2a, 2r** and **2u** has provided insight into their safety and potential use in pharmaceutical research. However, further experimental studies are needed to better understand the underlying mechanisms of toxicity and to optimize the compound design to improve their efficacy and safety.

4 Conclusions

Structural analogs of natural integrastatins with an epoxydibenzoxocine fragment are of great interest to researchers and pharmacists worldwide due to their broad spectrum of biological activity, including antiviral, antioxidant, antimicrobial, antifungal and antitumor activity. At the same time, *in silico* studies can be successfully used to predict numerous physicochemical and pharmacological properties of natural and synthetic biologically active molecules. In the present study, an in silico approach was used to comparatively evaluate

the pharmaceutical potential of a series of 21 novel integrastatin derivatives, previously synthesized but not characterized in terms of physicochemical and bioactive parameters.

Initially, the molecular structures of 21 studied compounds **2a-u** were subjected to the procedure of quantum-chemical geometry optimization and evaluation of the calculated parameters using DFT RB3LYP 6-311++G(d, p) CPCM (solvent — water) method with the help of the Gaussian 16 program. It was shown that all the studied compounds have a non-planar structure due to the presence of a chair-shaped structure of the central epoxybenzo[7,8]oxocine fragment. The global chemical reactivity descriptors of the compounds **2a-u** were estimated based on the HOMO and LUMO frontier orbitals characteristics. It was shown that compounds **2a-u** are characterized by a sufficiently large energy gap ΔE_{gap} from 3.8 to 4.6 eV, have a high ionization potential IP from 5.9 to 7.1 eV and an electron affinity *EA* value at a level of 2.1 to 3.2 eV. The molecular hardness η of the studied molecules **2a-u** varies from 1.7 to 2.3 eV, which, together with a fairly large energy gap, indicates the hard nature of the compounds. Analysis of the molecular electrostatic potential (MEP) of compounds **2a-u** showed that the nucleophilic center is located on the oxygen atom of the carbonyl, while the hydrogen atom of the pyridine is one of the most electrophilic centers. The applied complex quantum-chemical approach contributed to a deeper understanding of the electronic structure and molecular properties of the studied compounds **2a-u**, as well as the identification of their reaction centers and an assessment of the chemical potential for subsequent *in silico* studies of biological activity.

PASS Online resource was used for the assessment of potential biological activity of the studied compounds **2a-u**, which allowed to identify their antiviral potential and inhibitory potential as CYP2C19 inducers. These types of biological activity of compounds **2a-u** were further investigated using the molecular docking method for the efficiency of binding with HIV-1 (PDB ID: **3V81**), SARS-CoV-2 (PDB ID: **7AAP**) and CYP2C19 inducer (PDB ID: **4GQS**) proteins using AutoDock Vina tool. All 21 tested compounds showed high antiviral potential against Human immunodeficiency virus HIV-1 reverse transcriptase protein (PDB ID: **3V81**) and protein of the RNA-dependent RNA polymerase of the SARS-CoV-2 (PDB ID: **7AAP**), and ligand **2u** demonstrated the best binding to both viral proteins. The inhibitory potential of compounds **2a-u** as CYP2C19 inducers was also assessed by docking, and ligand **2r** demonstrated the highest binding affinity with **4GQS** protein.

At the final stage of the study, three representatives of the studied series of compounds — compounds **2a, 2r** and **2u** were subjected to *in silico* assessment of ADMET properties using ADMETlab 3.0 online portal. It was noted that all three studied compounds comply with Lipinski's Rule of Five, according to which they have a molecular weight less than 500 Da, a log*P* value less than 5, a number of hydrogen bond donors (nHD) no more than 5, a number of hydrogen bond acceptors (nHA) no more than 10, a topological polar surface area (TPSA) value less than 140 Å². The studied compounds **2a, 2r** and **2u** showed potentially good Caco2 permeability and good absorption in the human gastrointestinal tract, which indicates a potentially high oral efficiency. At the same time, compounds **2a, 2r** and **2u** demonstrated low potential for penetration through the blood-brain barrier and high potential for inhibition of the CYP2C19 enzyme. Evaluation of hematotoxicity and immunotoxicity of the studied compounds showed a promising safety profile for their therapeutic use.

In general, the complex *in silico* study of the properties of 21 new integrastatin derivatives showed their high potential as CYP2C19 inducers and high antiviral potential against HIV-1 and COVID-19 viruses, potentially high oral efficacy of pharmaceuticals based on them and a promising safety profile for their therapeutic use. However, further experimental *in vitro* and *in vivo* studies is need for more accurate evaluation the assumptions made on the basis of *in silico* approach, for better understanding of the underlying mechanisms of toxicity, pharmacokinetics, pharmacodynamics and side effects.

Supporting Information

The Supporting Information is available free at https://ejc.buketov.edu.kz/index.php/ejc/article/view/207/155

Funding

Author Information*

*The authors' names are presented in the following order: First Name, Middle Name and Last Name

Aida Sabitovna Rakhimzhanova — Assistant Professor, Department of Physical and Analytical Chemistry, Karaganda Buketov University, Universitetskaya street, 28, 100024, Karaganda, Kazakhstan; e-mail: aida_ekb@mail.ru, https://orcid.org/0000-0002-4984-623X

Ruslan Arslanovich Muzaparov — 2nd Year Master Student, Department of Physical and Analytical Chemistry, Karaganda Buketov University, Universitetskaya street, 28, 100024, Karaganda, Kazakhstan; e-mail: mega.muzaparov@mail.ru, https://orcid.org/0009-0005-4480-4355

Irina Anatolevna Pustolaikina (*corresponding author*) — Candidate of Chemical Sciences, Associate Professor, Department of Physical and Analytical Chemistry, Karaganda Buketov University, Universitetskaya street, 28, 100024, Karaganda, Kazakhstan; e-mail: ipustolaikina@gmail.com, https://orcid.org/0000-0001-6319-666

Alfiya Faridovna Kurmanova — Candidate of Chemical Sciences, Professor, Department of Physical and Analytical Chemistry, Karaganda Buketov University, Universitetskaya street, 28, 100024, Karaganda, Kazakhstan; e-mail: alfiya_kurmanova@mail.ru, https://orcid.org/0000-0003-4548-8145

Sergey Nikolaevich Nikolskiy — Doctor of Chemical Sciences, Full Professor, Department of Physical and Analytical Chemistry, Karaganda Buketov University, Universitetskaya street, 28, 100024, Karaganda, Kazakhstan; e-mail: sergeynikolsky@mail.ru; https://orcid.org/0000-0003-3175-6938

Darya Dmitrievna Kapishnikova — Student, Institute of Chemistry, Saint Petersburg State University, Universitetskii prospect, 26, 198504, Saint Petersburg, Russia; e-mail: st130421@student.spbu.ru, https://orcid.org/0009-0003-2129-9988

Alena Leonidovna Stalinskaya — Assistant, School of Natural Sciences, University of Tyumen, Tyumen, 15a Perekopskaya St., 625003, Russia; e-mail: a.l.stalinskaya@utmn.ru; https://orcid.org/0000-0002-2172-074X

Ivan Vyacheslavovich Kulakov — Doctor of Chemical Sciences, Associate Professor, Higher School of Natural Science, University of Tyumen, Tyumen, 15a Perekopskaya St., 625003, Russia; e-mail: i.v.kulakov@utmn.ru; https://orcid.org/0000-0001-5772-2096

Author Contributions

The manuscript was written through contributions of all authors. All authors have given approval to the final version of the manuscript. CRediT: **Aida Sabitovna Rakhimzhanova** investigation, formal analysis, visualization; **Ruslan Arslanovich Muzaparov** investigation, formal analysis, visualization; **Irina Anatolevna Pustolaikina** funding acquisition, project administration, supervision, methodology, validation, writing-review & editing; **Alfiya Faridovna Kurmanova** resources, data curation, validation; **Sergey Nikolaevich Nikolskiy** resources, software, data curation; **Darya Dmitrievna Kapishnikova** formal analysis, visualization; **Alena Leonidovna Stalinskaya** investigation, data curation, visualization; **Ivan Vyacheslavovich Kulakov** conceptualization, data curation, methodology, writing-original draft.

Conflicts of Interest

The authors declare no conflict of interest.

References

1   Kulakov, I. V., Stalinskaya, A. L., Chikunov, S. Y., & Gatilov, Y. V. (2021). Synthesis of new representatives of 11,12-dihydro-5H-5,11-epoxybenzo 7,8 oxocino 4,3-pyridines — structural analogues of integrastatins A, B. *New Journal of Chemistry*, *45*(7), 3559–3569. https://doi.org/10.1039/d0nj06117d

2 Singh, S. B., Pelaez, F., Hazuda, D. J., & Lingham, R. B. (2005). Discovery of natural product inhibitors of HIV-1 integrase at Merck. *Drugs Fut*, *30*(3), 277–299. https://doi.org/10.1358/dof.2005.030.03.885746

3 Singh, S. B., Zink, D. L., Quamina, D. S., Pelaez, F., Teran, A., Felock, P., & Hazuda, D. J. (2002). Integrastatins: structure and HIV-1 integrase inhibitory activities of two novel racemic tetracyclic aromatic heterocycles produced by two fungal species. *Tetrahedron Letters, 43*(13), 2351–2354. https://doi.org/10.1016/s0040-4039(02)00265-4

4 Johnson, A. A., Marchand, C., & Pommier, Y. (2004). HIV-1 integrase inhibitors: a decade of research and two drugs in clinical trial. *Current Topics in Medicinal Chemistry*, *4*(10), 1059–1077. https://doi.org/10.2174/1568026043388394

5 Foot, J. S., Giblin, G. M., & Taylor, R. J. (2003). Synthesis of the Integrastatin Nucleus Using the Ramberg−Bäcklund Reaction. *Organic Letters*, *5*(23), 4441–4444. https://doi.org/10.1021/ol035786v

6 Yamagiwa, Y., Haruna, N., Kawakami, H., & Matsumoto, K. (2020). Improved and Practical Synthesis of the Integrastatin Core. *Bulletin of the Chemical Society of Japan*, *93*(8), 1036–1042. https://doi.org/10.1246/bcsj.20200070

7 Tadross, P. M., Bugga, P., & Stoltz, B. M. (2011). A rapid and convergent synthesis of the integrastatin core. *Organic & biomolecular chemistry*, *9*(15), 5354–5357. https://doi.org/10.1039/c1ob05725a

8 More, A. A., & Ramana, C. V. (2016). o-Quinone methides via oxone-mediated benzofuran oxidative dearomatization and their intramolecular cycloaddition with carbonyl groups: an expeditious construction of the central tetracyclic core of integrastatins, Epicoccolide A, and Epicocconigrone A. *Organic letters*, *18*(3), 612–615. https://doi.org/10.1021/acs.orglett.5b03707

9 Ramana, C. V., Reddy, C. N., & Gonnade, R. G. (2008). An expeditious one-step entry to the tetracyclic core of integrastatins. *Chemical communications*, (27), 3151–3153. https://doi.org/10.1039/b801755g

10 Jeong, J. Y., Sperry, J., & Brimble, M. A. (2019). Synthesis of the Tetracyclic Cores of the Integrastatins, Epicoccolide A and Epicocconigrone A. *The Journal of Organic Chemistry*, *84*(18), 11935–11944. https://doi.org/10.1021/acs.joc.9b01796

11 More, A. A., & Ramana, C. V. (2016). Total synthesis of integrastatin B enabled by a benzofuran oxidative dearomatization cascade. *Organic letters*, *18*(6), 1458–1461. https://doi.org/10.1021/acs.orglett.6b00404

12 Stalinskaya, A. L., Martynenko, N. V., Shulgau, Z. T., Shustov, A. V., Keyer, V. V., & Kulakov, I. V. (2022). Synthesis and Antiviral Properties against SARS-CoV-2 of Epoxybenzooxocino 4,3-Pyridine Derivatives. *Molecules*, *27*(12), Article 3701. https://doi.org/10.3390/molecules27123701

13 Stalinskaya, A. L., Chikunov, S. Y., Pustolaikina, I. A., & Kulakov, I.V. (2022). Cyclization Reaction of 3,5-Diacetyl-2,6-dimethylpyridine with Salicylic Aldehyde and Its Derivatives: Quantum-Chemical Study and Molecular Docking. *Russian Journal of General Chemistry*, *92*(5), 914–924. https://doi.org/10.1134/s107036322205022x

14 Stalinskaya, A. L., Chikunov, S. Y., Pustolaikina, I. A., Gatilov, Y. V., Kulakov, I. V. (2023). Synthesis of New Structural Analogues of Natural Integrastatins with a Basic Epoxybenzo[7,8]oxocine Skeleton: Combined Experimental and Computational Study. *Synthesis*. https://doi.org/10.1055/s-0042-1751521

15 Bortolato, A., Perruccio, F., & Moro, S. (2011). Successful Applications of In silico Approaches for Lead/Drug Discovery. In silico Lead Discovery, 163–175. https://doi.org/10.2174/978160805142711101010163

16 Tian, S., Wang, J., Li, Y., Li, D., Xu, L., & Hou, T. (2015). The application of in silico drug-likeness predictions in pharmaceutical research. *Advanced drug delivery reviews*, *86*, 2–10. https://doi.org/10.1016/j.addr.2015.01.009

17 Aldossary, A., Campos-Gonzalez-Angulo, J. A., Pablo-García, S., Leong, S. X., Rajaonson, E. M., Thiede, L., ... & Aspuru-Guzik, A. (2024). In silico chemical experiments in the Age of AI: From quantum chemistry to machine learning and back. *Advanced Materials*, 2402369. https://doi.org/10.1002/adma.202402369

18 Paliwal, A., Jain, S., Kumar, S., Wal, P., Khandai, M., Khandige, P. S., ... & Srivastava, S. (2024). Predictive Modelling in pharmacokinetics: from in-silico simulations to personalized medicine. *Expert Opinion on Drug Metabolism & Toxicology*, *20*(4), 181–195. https://doi.org/10.1080/17425255.2024.2330666

19 Evans, D. A. (2014). History of the Harvard ChemDraw Project. Angewandte Chemie International Edition, *53*(42), 11140–11145. Portico. https://doi.org/10.1002/anie.201405820

20 van Gunsteren, W. F., & Oostenbrink, C. (2024). Methods for Classical-Mechanical Molecular Simulation in Chemistry: Achievements, Limitations, Perspectives. *Journal of Chemical Information and Modeling*, *64*(16), 6281–6304. https://doi.org/10.1021/acs.jcim.4c00823

21 Gaussian 16, Revision A.03, M.J. Frisch, G.W. Trucks, H.B. Schlegel, G.E. Scuseria, M.A. Robb, J.R. Cheeseman, G. Scalmani, V. Barone, G.A. Petersson, H. Nakatsuji, X. Li, M. Caricato, A.V. Marenich, J. Bloino, B.G. Janesko, R. Gomperts, B. Mennucci, H.P. Hratchian, J.V. Ortiz, A.F. Izmaylov, J.L. Sonnenberg, D. Williams-Young, F. Ding, F. Lipparini, F. Egidi, J. Goings, B. Peng, A. Petrone, T. Henderson, D. Ranasinghe, V.G. Zakrzewski, J. Gao, N. Rega, G. Zheng, W. Liang, M. Hada, M. Ehara, K. Toyota, R. Fukuda, J. Hasegawa, M. Ishida, T. Nakajima, Y. Honda, O. Kitao, H. Nakai, T. Vreven, K. Throssell, J.A. Montgomery, Jr., J.E. Peralta, F. Ogliaro, M.J. Bearpark, J.J. Heyd, E.N. Brothers, K.N. Kudin, V.N. Staroverov, T.A. Keith, R. Kobayashi, J. Normand, K. Raghavachari, A.P. Rendell, J.C. Burant, S.S. Iyengar, J. Tomasi, M. Cossi, J.M. Millam, M. Klene, C. Adamo, R. Cammi, J.W. Ochterski, R.L. Martin, K. Morokuma, O. Farkas, J.B. Foresman, and D.J. Fox, Gaussian, Inc., Wallingford CT, 2016.

22 Dennington, R., Keith, T., Millam, J. GaussView, Version 6. Semichem Inc., Shawnee Mission, KS, 2016. http://gaussian.com

23 Ipek, C., Gümüş, H., Şimşek, M., & Tosun, M. (2022). DFT and Molecular Docking Study of 1-(2′-Thiophen)-2-propen-1-one-3-(2,3,5-trichlorophenyl) (TTCP) Molecule as Antiviral to Covid-19 Main Protease. Arabian Journal for Science and Engineering, *48*(1), 1031–1040. https://doi.org/10.1007/s13369-022-07293-4

24 Rharmili, N., Sert, Y., Rodi, Y. K., Chahdi, F. O., Haoudi, A., Mague, J. T., ... & Sebbar, N. K. (2024). Synthesis of new N-alkylated 6-bromoindoline-2.3-dione derivatives: crystal structures, spectroscopic characterizations, Hirschfeld surface analyses, molecular docking studies, DFT calculations, and antibacterial activity. *Results in Chemistry*, *7*, 101338. https://doi.org/10.1016/j.rechem.2024.101338

25 Kulakov, I. V., Chikunov, S. Y., Pustolaikina, I. A., & Gatilov, Y. V. (2024). Synthesis of a New Heterocyclic System: Pyrimidine Structural Analogues of Natural Integrastatins A, B. *Synlett*, *35*(15), 1799–1806. https://doi.org/10.1055/a-2239-6657

26 Tomasi, J., Mennucci, B., & Cammi, R. (2005). Quantum Mechanical Continuum Solvation Models. *Chemical Reviews*, 105(8), 2999–3094. https://doi.org/10.1021/cr9904009

27 Schueuermann, G. (2004). Quantum Chemical Descriptors in Structure-Activity Relation-ships–Calculation, Interpretation, and Comparison of Methods. *Predicting chemical toxicity and fate*, 85–149. https://doi.org/10.1201/9780203642627-14

28 Filimonov, D., & Poroikov, V. (2008). Probabilistic Approaches in Activity Prediction. Chemoinformatics Approaches to Virtual Screening, 182–216. https://doi.org/10.1039/9781847558879-00182

29 Makiyah, S. N. N., Usman, S., & Ahkam, A. H. (2024). Molecular Docking Investigation of Dioscorea alata Compounds Binding to CCKBR, CHRM3, CHRM5, and H2R for Gastric Ulcer Treatment. *Trends in Sciences*, *21*(5), 7358–7358. https://doi.org/10.48048/tis.2024.7358

30 Sulimov, A. V., Ilin, I. S., Tashchilova, A. S., Kondakova, O. A., Kutov, D. C., & Sulimov, V. B. (2024). Docking and other computing tools in drug design against SARS-CoV-2. *SAR and QSAR in Environmental Research*, *35*(2), 91–136. https://doi.org/10.1080/1062936x.2024.2306336

31 Eberhardt, J., Santos-Martins, D., Tillack, A. F., & Forli, S. (2021). AutoDock Vina 1.2.0: New Docking Methods, Expanded Force Field, and Python Bindings. *Journal of Chemical Information and Modeling*, *61*(8), 3891–3898. https://doi.org/10.1021/acs.jcim.1c00203

32 Trott, O., & Olson, A. J. (2009). AutoDock Vina: Improving the speed and accuracy of docking with a new scoring function, efficient optimization, and multithreading. *Journal of Computational Chemistry, 31*(2), 455–461. Portico. https://doi.org/10.1002/jcc.21334

33 Berman, H.M., Westbrook, J., Feng, Z., Gilliland, G., Bhat, T.N., Weissig, H., Shindyalov, I.N., & Bourne, P.E. (2000). The Protein Data Bank Nucleic Acids Research 28: 235–242 https://doi.org/10.1093/nar/28.1.235

34 Das, K., Martinez, S.E., Arnold, E. (2011) Crystal structure of HIV-1 reverse transcriptase (RT) with DNA and the nonnucleoside inhibitor nevirapine. https://doi.org/10.2210/pdb3V81/pdb

35 Naydenova, K., Muir, K.W., Wu, L.F., Zhang, Z., Coscia, F., Peet, M., Castro-Hartman, P., Qian, P., Sader, K., Dent, K., Kimanius, D., Sutherland, J.D., Lowe, J., Barford, D., & Russo, C.J. (2020). Nsp7-Nsp8-Nsp12 SARS-CoV2 RNA-dependent RNA polymerase in complex with template:primer dsRNA and favipiravir-RTP. https://doi.org/10.2210/pdb7AAP/pdb

36 Reynald, R.L., Sansen, S., Stout, C.D., & Johnson, E.F. (2012). Structure of Human Microsomal Cytochrome P450 (CYP) 2C19. https://doi.org/10.2210/pdb4GQS/pdb

37 BIOVIA, Dassault Systèmes, BIOVIA Discovery Studio, Release 2021, Sand Diego: Dassault Systèmes, 2023.

38 Ekins, S., Lane, T. R., Urbina, F., & Puhl, A. C. (2024). In silico ADME/tox comes of age: twenty years later. *Xenobiotica*, *54*(7), 352–358. https://doi.org/10.1080/00498254.2023.2245049

39 Chen, M., Yang, J., Tang, C., Lu, X., Wei, Z., Liu, Y., ... & Li, H. (2024). Improving ADMET prediction accuracy for candidate drugs: Factors to consider in QSPR modeling approaches. *Current Topics in Medicinal Chemistry*, *24*(3), 222–242. https://doi.org/10.2174/0115680266280005231207105900

40 Wei, Y., Palazzolo, L., Mariem, O. B., Bianchi, D., Laurenzi, T., Guerrini, U., & Eberini, I. (2024). Investigation of in silico studies for cytochrome P450 isoforms specificity. *Computational and Structural Biotechnology Journal*. https://doi.org/10.1016/j.csbj.2024.08.002

41 Lohit, N., Singh, A. K., Kumar, A., Singh, H., Yadav, J. P., Singh, K., & Kumar, P. (2024). Description and In silico ADME Studies of US-FDA Approved Drugs or Drugs under Clinical Trial which Violate the Lipinski's Rule of 5. *Letters in Drug Design & Discovery*, *21*(8), 1334–1358. https://doi.org/10.2174/1570180820666230224112505

42 Pereira, G. C. (2020). Computational Approaches in Drug Development and Phytocompound Analysis. Plant-Derived Bioactives, 529–548. https://doi.org/10.1007/978-981-15-2361-8_24

43 Sohail, A., & Li, Z. (2018). Computational Approaches in Biomedical Nanoengineering: An Overview. Computational Approaches in Biomedical Nano-Engineering, 1–22. Portico. https://doi.org/10.1002/9783527344758.ch1